Supporting Information

Rational construction of core-shell Ni_3S_2@$Ni(OH)_2$ nanostructure as the battery-like electrode for supercapacitors

Jinghuang Lin, Xiaohang Zheng*, Yiheng Wang, Haoyan Liang, Henan Jia, Shulin Chen, Junlei Qi*, Jian Cao*, Weidong Fei and Jicai Feng

State Key Laboratory of Advanced Welding and Joining, Harbin Institute of Technology, Harbin 150001, China

*Corresponding authors: Tel. /fax: 86-451-86418146;

E-mail: jlqi@hit.edu.cn (J. Qi)

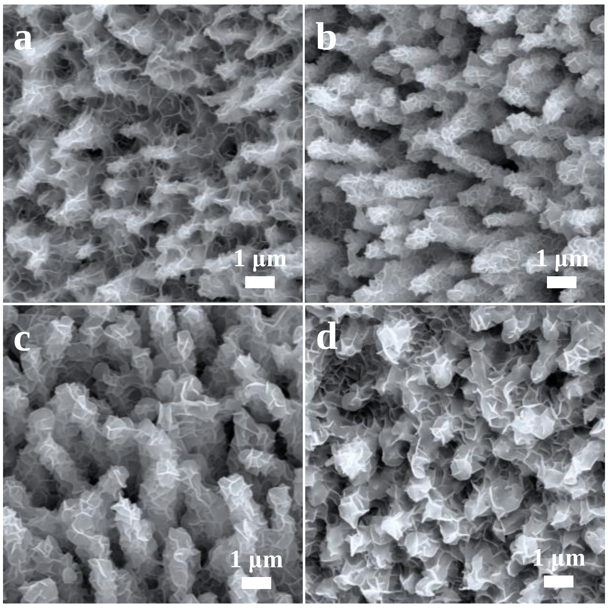

Fig. S1 SEM images of Ni_3S_2@$Ni(OH)_2$ samples with different immersion time: (a) 5 min, (b) 10min, (c) 15 min, (d) 20 min.

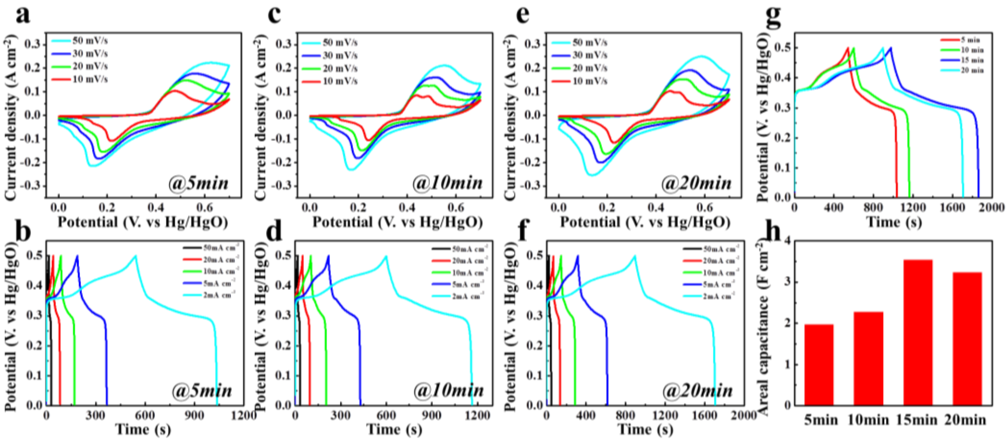

Fig. S2 CV and GCD curves of Ni_3S_2@$Ni(OH)_2$ samples with different immersion time: (a, b) 5min, (c, d) 10 min and (e, f) 20min. (g) The GCD curves at a current density of 2 mA cm^{-2} for Ni_3S_2@$Ni(OH)_2$ samples with different immersion time. (h) The areal capacitance of Ni_3S_2@$Ni(OH)_2$ samples with different immersion time at 2 mA cm^{-2}.

For comparison, Ni_3S_2@$Ni(OH)_2$ samples with different immersion time (5, 10, 15, 20 min) also prepared. Firstly, the electrochemical performances of Ni_3S_2@$Ni(OH)_2$ samples with different immersion time (5, 10, 15, 20 min) were compared. **Fig. S1** shows the SEM images of Ni_3S_2@$Ni(OH)_2$ samples with different immersion time. As the immersion time increases, the surface of Ni_3S_2 nanorods is gradually covered by $Ni(OH)_2$ nanosheets. Undoubtedly, the size of $Ni(OH)_2$ nanosheets as shell can be adjusted by controlling the immersion time. **Fig. S2g** shows the GCD curves of Ni_3S_2@$Ni(OH)_2$ samples with different immersion time. Obviously, Ni_3S_2@$Ni(OH)_2$-15min electrode showed the longest discharge time at 2 mA cm^{-2}, indicating the highest specific capacitance. According to the above results, the following performance tests and discussion were focused on the Ni_3S_2@$Ni(OH)_2$ obtained with 15 min immersion time.

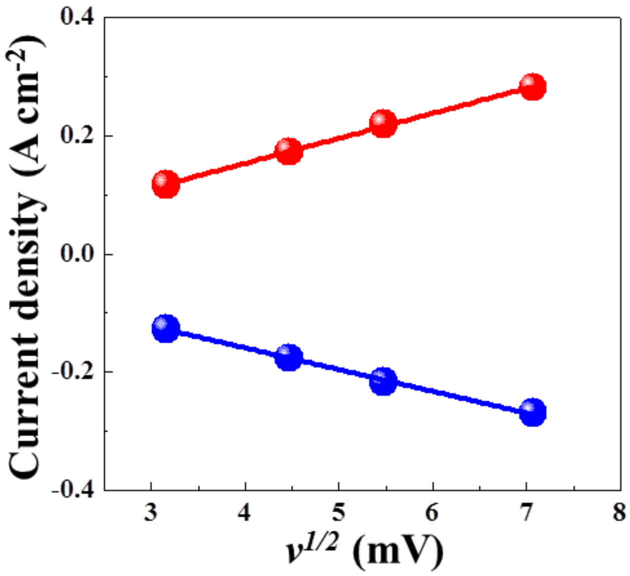

Fig. S3 The corresponding current density (i)–$v^{1/2}$ (scan rate$^{1/2}$) plots of $Ni_3S_2@Ni(OH)_2$

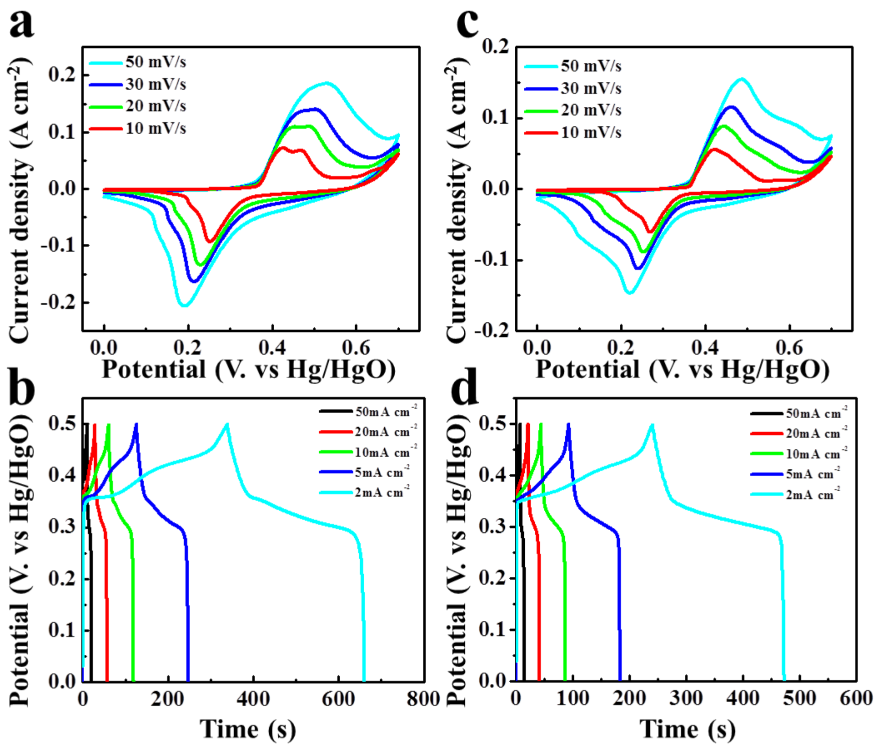

Fig. S4 CV and GCD curves of (a, b) Ni_3S_2 and (c, d) $Ni(OH)_2$.

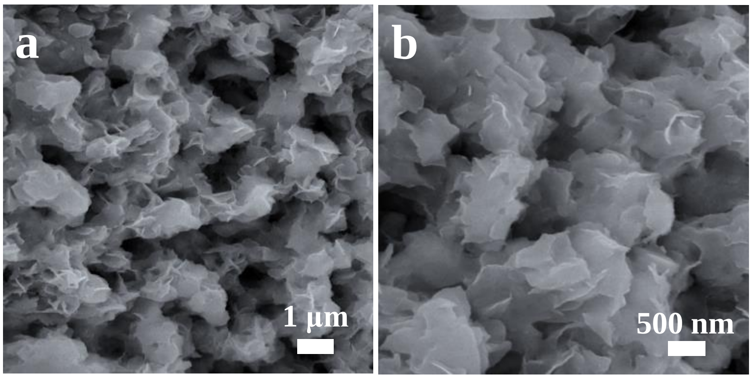

Fig. S5 SEM images of $Ni_3S_2@Ni(OH)_2$ after 10000 cycles.

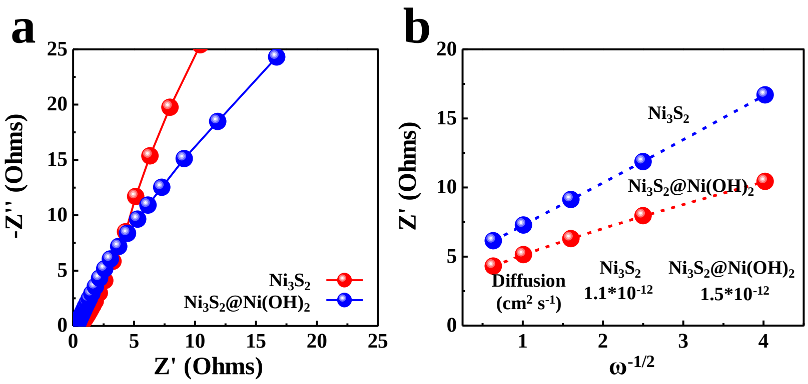

Fig. S6 The relationship between Z' and $\omega^{-1/2}$ in the low-frequency region of $Ni_3S_2@Ni(OH)_2$ and Ni_3S_2.

According to previous researches [1-4], the OH^- ion diffusion coefficient (D_{OH}^-, cm^2 s^{-1}) was calculated by following equation:

$$D_{OH}^- = (RT)^2/2(A\,n^2F^2C_{OH}^-\sigma)^2$$

where R, T, A, n, F, C_{OH}^- and σ represent the gas constant, absolute temperature, electrode area, number of electrons transfer, Faraday constant, the OH^- concentration and Warburg factor. And σ could be calculated by the slope of line in the low frequency region, according to the following equation [4,5]:

$$Z' = R_e + R_{ct} + \sigma$$

Based on above equation, the D_{OH}^- has been calculated and the results are shown in Fig. S6. As a results, the calculated D_{OH}^- of $Ni_3S_2@Ni(OH)_2$ is larger than that of pristine Ni_3S_2, suggesting the faster ion transport.

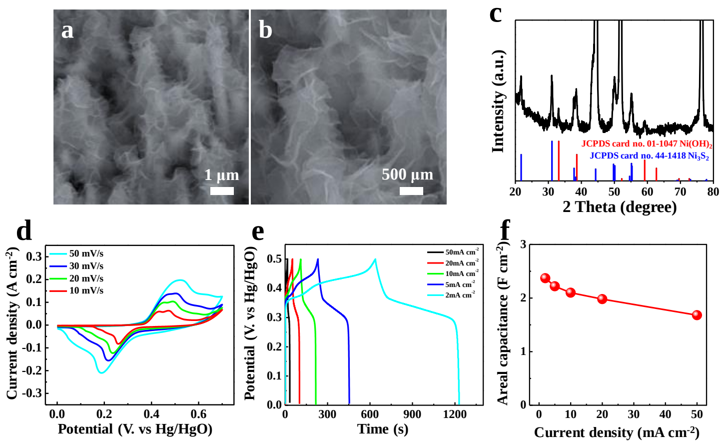

Fig. S7 (a,b) SEM images of Ni_3S_2@$Ni(OH)_2$-Ar. (c) XRD pattern of Ni_3S_2@$Ni(OH)_2$-Ar. (d-f) CV, GCD curves and corresponding areal capacitance of Ni_3S_2@$Ni(OH)_2$-Ar.

In order to investigate influence of crystallinity on the electrochemical performances, the obtained Ni_3S_2@$Ni(OH)_2$ was annealed at Ar atmosphere in 150 ^{o}C for 2h (labeled as Ni_3S_2@$Ni(OH)_2$-Ar). As shown in Fig. S7a-b, SEM images suggested that the morphology and structure of Ni_3S_2@$Ni(OH)_2$-Ar show no obvious changes. As shown in Fig. S7c, XRD result shows that the peaks of $Ni(OH)_2$ become obvious and sharp after annealing process, suggesting the improvement of crystallinity of the $Ni(OH)_2$. Fig. S7d-S7f show the electrochemical performance of Ni_3S_2@$Ni(OH)_2$-Ar. As a results, Ni_3S_2@$Ni(OH)_2$-Ar shows the lower capacitance than that of pristine Ni_3S_2@$Ni(OH)_2$, only 2.37 F cm^{-2} at 2 mA cm^{-2}. According to previous results [6-8], electrodes with low crystallinity could be able to achieve better electrochemical performances than that of crystalline counterparts, due to more structure disorder and defects.

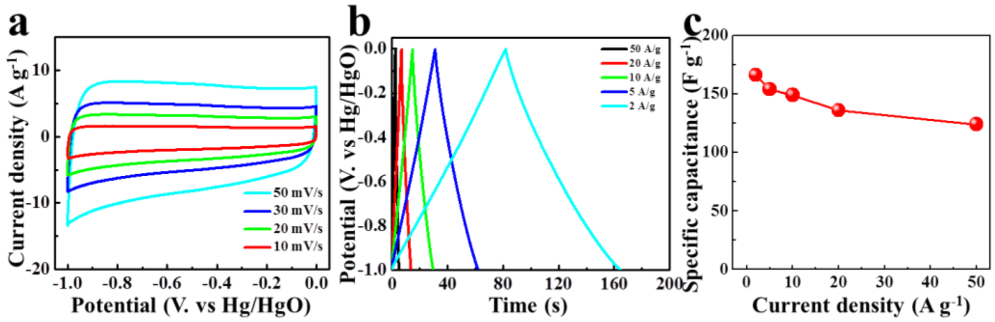

Fig. S8 (a and b) CV and GCD curves of AC at various scan rate and (b) corresponding specific capacitance

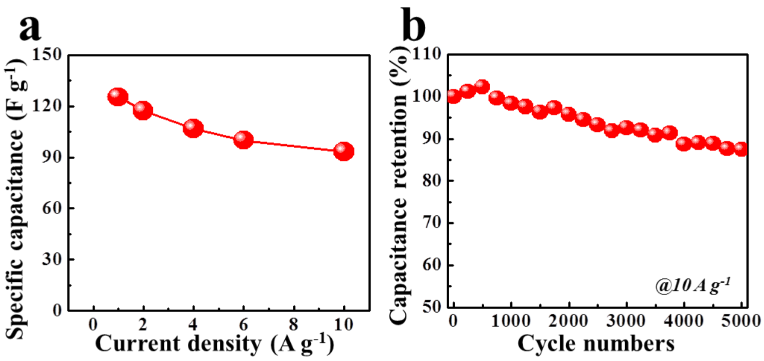

Fig. S9 (a) The specific capacitance *vs.* current density of Ni_3S_2@$Ni(OH)_2$//AC, (b) Cycling performance of Ni_3S_2@$Ni(OH)_2$//AC, which was determined by GCD tests at the current density of 10 A g^{-1} for 5000 cycles.

Table S1 The specific capacitance of various electrodes in the three-electrode system in references

Electrode materials	**Electrolyte**	**Specific capacitance**	**Potential Windows (V)**	**Reference**
Surface-enriched Ni-Co-S/Graphene	6 M KOH	1436 F g^{-1}	-0.05-0.55	9
Ni_3S_2@β-NiS	6 M KOH	1158 F g^{-1}	-0.2-0.5	10
nickel sulfides/MoS_2-CNT	3 M KOH	757 F g^{-1}	0-0.55	11
NiS_2 hollow sphere	2 M KOH	1643 F g^{-1}	0-0.7	12
Ni_3S_2@CdS	3 M KOH	3.15 F cm^{-2}	0-0.5	13
NiS nanosheets array	1 M NaOH	1325 F g^{-1}	0-0.8	14
NiS/carbon aerogle	2 M KOH	1606 F g^{-1}	0-0.5	15
graphene-wrapped nickel sul-fide nanoprisms	2 M KOH	1495 F g^{-1}	0-0.5	16
$NiMoO_4$@Ni-Co-S	2 M KOH	2.27 F cm^{-2}	0-0.65	17
Co_3O_4@CdS	3 M KOH	1539 F g^{-1}	0-0.6	18
hierarchical carbon@Ni_3S_2@MoS2	6 M KOH	1544 F g^{-1}	0-0.4	19
Ni_3S_2@$Ni(OH)_2$	6M KOH	1775 F g^{-1} (3.55 F cm^{-2})	0-0.5	This work

Reference:

1. X. Zhao, W. Cai, Y. Yang, X. Song, Z. Neale, H. Wang, J. Sui and G. Cao, *Nano Energy*, 2018, **47**, 224-234.

2. X. Zhao, H. Wang, J. Cao, W. Cai and J. Sui, *Chem. Commun.*, 2017, **53**, 10723-10726.

3. C. Liu, R. Massé, X. Nan and G. Cao, *Energy Storage Mater.*, 2016, **4**, 15-58.

4. T. F. Yi, Y. Xie, L.J. Jiang, J. Shu, C. B. Yue, A. N. Zhou and M. F. Y, *RSC Adv.*, 2012, 2, 3541-3547.

5. S. Sarkar, H. Banda, and S. Mitra, *Electrochim. Acta*, 2013, **99**, 242-252.

6. J. Lang, L. Kong, W. Wu, Y. Luo and L. Kang, Chem. Commun., 2008, 4213-4215.

7. J. Chen, H. Wang, J. Deng, C. Xu and Y. Wang, J. Mater. Chem. A, 2018, 6, 8986-8991.

8. K. A. Owusu, L. Qu, J. Li, Z. Wang, K. Zhao, C. Yang, K. M. Hercule, C. Lin, C. Shi, Q. Wei, L. Zhou and L. Mai, Nat. Commun., 2017, 8, 14264–14275.

9. X. Wang, S. Zhao, L. Dong, Q. Lu, J. Zhu and C. Nan, *Energy Storage Mater.*, 2017, **6**, 180-187.

10. W. Li, S. Wang, L. Xin, M. Wu and X. Lou, *J. Mater. Chem. A*, 2016, **4**, 7700-7709.

11. X. Yang, L. Zhao and J. Lian, *J. Power Sources*, 2017, **343**, 373-382.

12. M. Lu, X. Yuan, X. Guan and G. Wang, *J. Mater. Chem. A*, 2017, **5**, 3621-3627.

13. X. Wang, B. Shi, Y. Fang, F. Rong, F. Huang, R. Que and M. Shao, *J. Mater. Chem. A*, 2017, **5**, 7165–7172.

14. N. Nair and B.R. Sankapal, *New J. Chem.*, 2016, **40**, 10144-10152.

15. L. Zuo, W. Fan, Y. Zhang, Y. Huang, W. Gao and T. Liu, *Nanoscale*, 2017, **9**, 4445-4455.

16. A. A. AbdelHamid, X. Yang, J. Yang, X. Chen and J. Y. Ying, *Nano Energy*, 2016, **26**, 425-437.

17. C. Chen, D. Yan, X. Luo, W. Gao, G. Huang, Z. Han, Y. Zeng and Z. Zhu, *ACS Appl. Mater. Interfaces*, 2018, **10**, 4662-4671.

18. D. S. Patil, S. A. Pawar and J. C. Shin, *Chem. Eng. J.*, 2018, **335**, 693-702.

19. L. Li, H. Yang, J. Yang, L. Zhang, J. Miao, Y. Zhang, C. Sun, W. Huang, X. Dong and B. Liu, *J. Mater. Chem. A*, 2016, **4**, 1319–1325.